JOURNAL OF GUIDANCE, CONTROL, AND DYNAMICS
Vol. 15, No. 3, May-June 1992

Autonomous Spacecraft Navigation and Control for Comet Landing

J. de Lafontaine*
European Space Agency, 2200 AG, Noordwijk Z-H, The Netherlands

The autonomous guidance, navigation, and control operations during the landing phase of the Comet Nucleus Sample Return mission are described and the associated performance of the onboard system is analyzed in terms of landing accuracy and relative velocity at touchdown. Two descent scenarios are developed and investigated: a slow descent strategy that optimizes the operation of an onboard laser mapper and a fast descent strategy that relies only on microwave measurements for navigation. It is demonstrated by means of Monte Carlo simulations that the first scenario provides a more accurate landing, whereas the second one is a suitable alternative to the case where the complex laser system has failed. Equatorial and polar descent orbits to a landing site on the comet equator are considered. Models of the comet, spacecraft dynamics, and instrument measurements are described, and the main features of the onboard algorithms are outlined. These models and algorithms are incorporated into a simulation software that is used to generate typical time histories of the spacecraft dynamical state during the landing phase.

Introduction

FUTURE missions described in the European Space Agency (ESA) space science program include deep-space missions requiring spacecraft on interplanetary flights to rendezvous and land on planetary bodies. One of the four cornerstones of the program, the Comet Nucleus Sample Return (CNSR) mission, has the objective of returning a comet nucleus sample to Earth laboratories, preserving its fundamental physical and chemical properties. It is believed that the laboratory analysis of cometary material will provide answers to questions related to the origin and early evolution of the solar system and the nature of its most primitive organic compounds. This search for the origin of the solar system explains the official name of the mission, Rosetta, in reference to the Rosetta Stone, which provided the key to the understanding of the hieroglyphics. The Rosetta mission is being studied jointly by the European Space Agency and NASA.

The eight-year mission involves an Earth gravity-assist maneuver two years after launch to inject the spacecraft on an interplanetary cruise to the aphelion of a short-period comet, where nucleus activity is low. After detection of the comet by the onboard cameras, a series of ground-commanded rendezvous maneuvers will bring the spacecraft in an orbit around the comet, some tens to a few hundreds of kilometers above it. A global mapping of the comet will identify scientifically interesting areas that are safe for landing. A closer observation of these candidate landing sites (from 5 to 15 km) will provide the high-resolution topographic and scientific measurements necessary for the selection of the most suitable one. Because of the long round-trip signal time to planetary bodies of interest (about 100 min to a comet at 6 AU), the descent and landing operations will be performed autonomously by the spacecraft. After spacecraft anchoring to the surface and drilling operations to acquire about 10 kg of cometary material, the spacecraft will take off for its return journey to Earth. An Earth reentry capsule containing the samples will separate from the main spacecraft platform a few days before it undergoes an aeroassisted braking and a parachute descent to the sea for recovery.

The baseline spacecraft is composed of three modules: the Cruiser, which provides the main spacecraft resources; the Lander, which supports the landing and drilling operations on the comet; and the Earth Re-Entry Vehicle, which provides the stable temperature environment for the preservation of the samples during the return cruise and atmospheric re-entry. The NASA Mariner Mark II spacecraft is currently baselined for the Cruiser module. The navigation instruments—gyros, star and target tracker, cameras, radar system, and laser mapper—are mounted on its high precision scan platform (HPSP), which is gimballed along two axes with respect to the main spacecraft body. Control actions are realized by reaction wheels, hydrazine thrusters (for attitude and small orbital maneuvers), cold gas thrusters (to avoid comet contamination during descent and touchdown), and a 400-N bipropellant main engine for large maneuvers.

This paper is primarily concerned with the descent and landing phase of the mission where onboard autonomy is required to perform the guidance, navigation, and control (GNC) functions. A previous analysis[1] of the Rosetta descent and landing has looked at the open-loop navigation problem in which the actions of the onboard GNC system are not considered. The purpose of the present work is to describe these onboard functions, to define the associated GNC system, and to quantify the performance of the closed-loop system. Graphical tools are developed and used to design descent and landing strategies, and the relative merits of these strategies are compared in terms of system complexity, accuracy (dispersion at landing), and safety (vertical and horizontal velocity at touchdown).

Mission Requirements and Constraints

The major differences between the Rosetta mission and previous autonomous landing missions on planetary bodies can be summarized as follows: 1) the irregular and largely unknown environment of a comet, 2) the requirement for a precise landing, and 3) the time constraints imposed by the return launch window. A rather poor a priori knowledge of the comet environment will be available before the actual encounter. The weak comet gravity field (5-500 μg at the surface) is expected to be irregular, with gravitational harmonics as important as the fundamental term. The surface may also present large irregularities (peaks, slope, cavities), perturbing the onboard microwave measurements and adding hazards to the landing. In this inhospitable environment, the requirement

Presented as Paper 90-2911 at the AIAA/AAS Astrodynamics Conference, Portland, OR, Aug. 20-22, 1990; received Feb. 12, 1991; revision received July 3, 1991; accepted for publication July 5, 1991.

*Control Systems Engineer, European Space Research and Technology Centre, Automation and Informatics Department, Postbus 299. Member AIAA.

for a precise landing will primarily ensure touchdown at a safe site, preselected by the ground during the observation phase of the mission. Landing accuracy will also improve the quality of the scientific returns by ensuring the acquisition of comet samples in specifically chosen areas (e.g., ice). Finally, unlike previous and currently planned fly-by and orbital missions to comets, the Rosetta mission is constrained by the return flight to Earth, implying a maximum of 100–200 days for the near- and on-comet operations. This constraint translates into a limited amount of time available to characterize the comet and estimate the parameters that are required to successfully achieve the scientific and engineering objectives of the mission.

One of the critical tasks of the ground navigation activities before landing will be to identify and quantify the parameters that are required for safe and accurate GNC operations. This navigation process involves not only an accurate ground reconstitution of the spacecraft motion relative to the comet but also an identification of the comet kinematic, dynamic, geometric, and topographic characteristics. The results of this ground activity will be uplinked to the spacecraft before autonomous descent and landing maneuvers are initiated. The onboard GNC system will then propagate its estimated dynamical state, using a simplified model of the environment complemented with measurements relative to inertial and comet-fixed references. A description of these models and measurements is now presented before their use in a simulation software is discussed. Both the real-world models used in the environment simulator and their simplified versions used in the onboard GNC emulator are described.

Comet Models

As a result of our poor initial knowledge of the comet characteristics, the study of the GNC system performance must take into account the large range of comet parameters that are shown in Table 1. The mean density and mean radius are used to compute the comet mass and the main term of the gravity field. In order to represent the irregular shape and gravity field expected of most comets, refinements to these mean properties will be introduced later. The onboard GNC system will benefit from about 40 days of comet observation and ground-based navigation to obtain a better knowledge of the spacecraft and comet states. Previous studies[1-4] dedicated to the Tempel 2, Comet Rendezvous Asteroid Flyby (CRAF), and Rosetta missions have addressed this navigation problem and their results will be used as a starting point in this paper. Because these studies rely on a wide range of different assumptions (frequency, accuracy and types of measurements, comet size and mass, initial estimation errors, observation interval, etc.), a correspondingly wide variation in the estimated parameters results. An attempt was made to select those that are more closely related to the scenario studied in this paper and the results are given in Table 2. It must be noted that the real-world models of the environment simulator described here do not have to exhibit the full complexity of the models normally assumed in these navigation studies. The descent and landing scenarios investigated here are not concerned with the estimation of the parameters of these models but only with the simulation of realistic differences between reality and what the onboard system knows about reality.

Gravity Field

From the navigation studies,[1-3] the accuracy in the knowledge of the comet gravitational parameter is between 0.01 and 0.4% (1σ). A value of 0.1% has been assumed here. In order to illustrate the impacts of an inaccurate onboard gravity model during the relatively short duration of the descent and landing operations discussed in this paper, a simple dipolar model has been adopted. The real-world model is composed of two mascons, each representing 50% of the total comet mass, and separated by one comet radius. The coordinates of these mascons are expressed in the comet-fixed kinematic frame (along principal inertia axes), with origin at the center of mass. The onboard gravitational model assumes a spherical gravity field.

Comet Kinematics

The orientation of the comet spin axis is determined by its right ascension ψ and inclination θ with respect to the inertial (ecliptic) frame. The comet may not spin exactly about its principal axis of maximum inertia because of possible outgassing torques and residual nutation from the perihelion passage, where these torques are important. However, the two comet angles ψ and θ are assumed to be constant over the short simulation intervals considered here. The spin initial phase ϕ_o and rate $\omega_c = \dot{\phi}$ complete the description of the comet kinematics. Since the maximum comet period of 3 h shown in Table 1 results in negative effective gravity for the low-density comets (centrifugal acceleration greater than gravitational acceleration at the surface), the 10-h period is a more realistic figure, which will be assumed throughout this paper.

The expected accuracy in the knowledge of these parameters depends on the orientation of the orbit and the availability of unambiguous surface landmarks that are tracked by the onboard cameras and processed on ground. Typical 1σ accuracies[1] are shown in Table 2.

Comet Shape

The purpose of a comet shape model is to represent the effects of comet nonsphericity on the radar and laser measurements. The large-scale effects are introduced with an ellipsoid comet shape, whereas the impact of local surface irregularities in the beamwidth of the instrument are accounted for directly in the instrument model as noise. The semimajor axes of the ellipsoid are chosen as follows: one at 120% of the mean radius (Table 1), the other at 80%, and the third one so as to keep the same total volume of a sphere with this mean radius (i.e., 104.2%). The ellipsoid is expressed in a geometric reference frame with origin and orientation that are not necessarily coincident with those of the kinematic frame in which the comet gravity field is expressed. The relative orientation of these two frames is not as important as their relative offset

Table 1 Comet properties

Parameters	Minimum	Typical	Maximum
Density, g/cm^3	0.2	1.0	1.5
Radius, m	1000	2500	10,000
Spin period, h	3	10	∞

Table 2 Comet model

Parameters	Real world; nominal	Onboard knowledge, 1σ
Mass, kg		
Minimum	8.38×10^{11}	0.1% of nominal
Typical	6.54×10^{13}	
Maximum	6.28×10^{15}	
Gravity field	dipolar	spherical
Kinematics[a]		
ψ	0 deg	0.077 deg
θ	45 deg	0.056 deg
ϕ_o	0 deg	0.082 deg
ω_c	1.75×10^{-4} rad/s	0.01%
Shape	ellipsoid	sphere
Geometric center	1% of radius offset from center of mass	coincident with center of mass
Landing site		
Latitude	0 deg	10-m error
Longitude	0 deg	in three axes

[a]Nominal comet attitude angles chosen arbitrarily.

(between the comet geometric and gravitational centers), for which a distance of 1% of the radius is assumed in the environmental simulator. On other other hand, the onboard GNC software assumes a simpler shape model: a spherical comet shape with coincident geometric and mass centers.

Landing Site

The inertial coordinates of the landing site are determined in the ground-based navigation process to an accuracy of 5–20 m.[1-3] An uncertainty of 10 m is assumed here. This value only takes into account the initial position error at the time when the deorbit parameters are uplinked to the spacecraft. These inertial coordinates are then propagated in time according to the onboard knowledge of the comet kinematics, thereby adding propagation errors to these initial estimates. In the simulations, the landing site will be located at the comet equator to maximize the effects of comet kinematics.

Spacecraft Dynamics Model

The spacecraft mass at the time of the deorbit maneuver is expected to be around 2000 kg. The onboard knowledge of this parameter (combined with the thrust magnitude uncertainty) is taken as 1% (1σ). Nongravitational accelerations caused by solar radiation pressure and attitude control thruster leaks are modeled in the simulator. Their magnitude is shown in Table 3. Their relatively long correlation times ($\sim$ days) make them appear basically as constant biases during the short duration of the descent and landing operations.

In the present simulations, only the translational motion of the spacecraft is numerically integrated. The effects of attitude motion on the pointing of sensors and actuators are modeled by bias and random errors with respect to their nominal pointing directions. The pointing accuracy of the Mariner Mark II HPSP is of the order of 2 mrad or 0.11 deg. Half of this value is taken as a fixed bias and the other half will represent 1σ random variations. These pointing errors affect the laser mapper and radar system mounted on the scan platform. The pointing of the body-mounted thrusters is determined by the attitude of the whole spacecraft with assumed errors of 0.5-deg bias and 0.5-deg 1σ random.

Onboard Instruments Model

The measurement of the spacecraft position and velocity relative to the comet surface is performed with a radar system and a laser mapper, both mounted on the scan platform. These instruments also measure the spacecraft orientation relative to the comet surface to ensure an upright attitude at touchdown. By processing of the radar and laser signals, it is possible to estimate the surface roughness so that dangerous landing areas can be avoided. The characteristics of these instruments are derived from the results of industrial studies[5,6] sponsored by ESA and they are summarized in Table 4. Some additional technical details are presented in the following.

Table 3 Spacecraft dynamics model

Parameters	Real world	Onboard knowledge
Spacecraft mass, kg	2000	1% (1σ)
ACS[a] gas leaks, m/s^2		
Bias	4×10^{-9}	—
Random, 1σ	4×10^{-10}	—
Solar pressure, m/s^2		
Bias	2×10^{-9}	—
Random, 1σ	2×10^{-10}	—
Platform pointing		to landing site
Bias	0.05 deg	
Random, 1σ	0.05 deg	
Spacecraft attitude		along surface normal
Bias	0.50 deg	
Random, 1σ	0.50 deg	

[a]Attitude control system.

Table 4 Spacecraft instruments (1σ values where applicable)

Radar system	
Pointing accuracy	
Bias	0.05 deg
Random	0.05 deg
Range accuracy	
Bias	5 m
Random	1% of range
Range rate accuracy	
Bias	5 mm/s
Random	5 mm/s
Beam width	0.4 deg
Squint angle	2 deg
Update frequency	1 Hz
Laser mapper	
Pointing accuracy	
Bias	0.05 deg
Random	0.05 deg
Mapping accuracy	
Bias	5 m
Random	5 m
Beam footprint (at 15 km)	60 cm
Field of view	± 4 deg
Pulse repetition frequency	400 Hz
Map update period (30 m subarea)	200 s
Accelerometers	
Measurement accuracy	1×10^{-7} m/s^2
Thrusters	
Thrust magnitude	
Main engine	400 N
Hydrazine/cold gas	10 N/30 N
Knowledge (before descent)	1% of nominal
Thrust direction error	
Bias	0.50 deg
Random	0.50 deg

The radar system[5] combines both the range and Doppler measurements. The half-meter antenna has four beams, one directed along the boresight and the three others squinted at 2 deg. At large distances from the comet (up to 200 km), the boresight beam provides range measurements. At a lower range (below 2–3 km), the three offset beams provide range and range rate measurements in three independent directions. With the three range measurements, the normal to the comet surface is derived, thus providing a two-axis relative attitude measurement. From the range rate measurements, the relative spacecraft velocity in three axes is computed. The radar instrument model, quantified in Table 4, takes into account the pointing error of the instrument, its measurement error, its sampling frequency, and the processing necessary to arrive at the velocity and normal measurements. The effect of surface asperities in the beam footprint are included in the random measurement errors.

The radar can observe only four of the six translational state variables of the spacecraft. For an accurate landing, the additional measurement of horizontal position relative to the landing site is necessary. Various techniques have been investigated to provide these measurements: 1) natural optical landmarks, 2) artificial landmarks (ejected by the spacecraft), and 3) elevation maps. Although the mathematical modeling is basically the same for all three measurement strategies, the one associated with the elevation maps, as derived from laser range measurements, has been adopted for the following reasons. Natural landmark tracking, although feasible on ground with human assistance and off-line image processing, becomes quite demanding for real-time autonomous operations in an unknown environment where low and varying lighting conditions exist. Artificial landmarks introduce mass penalties at launch and complex deployment maneuvers for their ejection

and accurate delivery to the comet surface. Elevation-map correlation techniques, on the other hand, appear more promising, and similar techniques have already been successfully applied in other fields. In addition to its horizontal navigation capability, the laser mapper provides redundancy to the radar functions (range and relative attitude).

The operational strategy of the laser mapper is the following. During the global and detailed mapping phase of the mission, topographic maps of the landing site (500 × 500 m) will be developed on ground using all of the available onboard measurements (passive optical, microwave, and laser). This map will be stored in the onboard computer before descent initiation. During the autonomous guided phase of the descent, the laser system will scan a subarea of about 30-m radius, correct these range measurements for attitude and range variations, and correlate them with the stored map in order to derive the relative position. The fine scanning of the laser beam is achieved with rotating wedges in the object space of the telescope. This design allows high scan rates but at the expense of restrictions on the size of the field of view. Preliminary design considerations[5] have arrived at a circular field of view of 4 deg (half cone). As a result, the 30-m-radius mapping area will be reachable above an altitude of 500 m.

The design of the laser mapper is still ongoing and its performance characteristics are still being refined. Other ESA studies are also investigating the performance of the associated onboard processing of the digital elevation maps. For the purpose of the present analysis, it is assumed that the map measurement errors are 5-m bias and 5-m random (1σ) (see Table 4). Since the measurement is obtained in instrument axes, the pointing errors induced by the platform are also accounted for in the simulation model. Finally, assuming that the real-time maps are constructed with one range measurement in every 20- × 20-cm horizontal cell on the comet surface at a pulse repetition frequency of 400 Hz, a minimum of 200 s is necessary to obtain a single horizontal position measurement. This operational constraint is taken into account in the closed-loop simulations presented later.

The thruster model is a pulse-width modulator that takes into account the minimum impulse bit of the thrusters and errors in the magnitude and direction of the thrust vector (due to misalignment and attitude errors). Onboard knowledge of the thruster forces before descent initiation are assumed to be 1% of nominal. Acceleration measurements during delta-v maneuvers are provided by three-axis accelerometers.

Descent Scenario

A planar representation of the descent scenario is illustrated in Fig. 1. The three trajectories shown correspond to the three main phases of the descent: 1) descent preparation, 2) homing, and 3) final or guided descent. The first two phases are separated by the deorbit maneuver and the last two by the synchronization maneuver. Note that Fig. 1 is a simplifed diagram; the homing orbit is shown as an ellipse; depending on the comet mass, it can be hyperbolic. In the figure, the homing orbit does not intersect the comet surface; in some cases, it will. Finally, all three trajectories are shown in the same plane for simplicity; in practice, each maneuver may involve a plane change, depending on mission constraints and landing site location.

Since this paper is not concerned with the design of optimal descent preparation and homing orbits (a mission analysis problem) but only with the autonomous final descent and the derivation of realistic dispersion and estimation errors at landing, typical—and not necessarily optimal—parameters for these orbits are first derived. Next, the spacecraft actual and estimated states are propagated along these orbits and along the final descent trajectory until touchdown.

Descent Preparation Orbit

This orbit is used to achieve the relative phasing of the spacecraft with the landing site while intensive ground tracking accurately reconstructs the dynamical state of the spacecraft. After one or two revolutions on this orbit, the deorbit maneuver commands, along with the results of the ground identification process, are uplinked to the spacecraft and the deorbit maneuver is executed at the preselected time.

The design of this orbit is constrained by the requirements of continuous visibility to the Earth for communication, an orbital period compatible with the convergence of the orbit determination estimation, a safe periapsis, and visibility to the

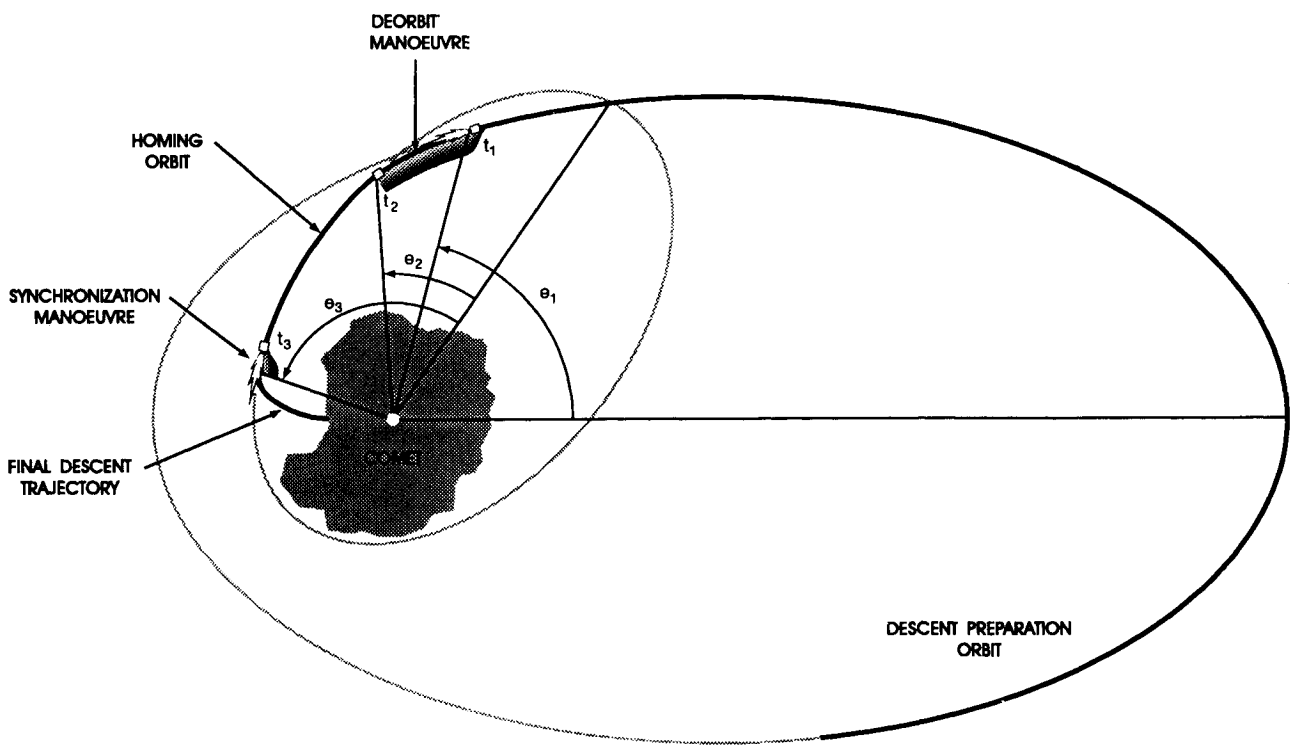

Fig. 1 Rosetta descent scenario.

landing site. Preliminary analyses show that a safe periapsis altitude of 3 km and an apoapsis altitude of 15 km are typical values for this orbit. Its orientation in inertial space is of secondary importance in the dispersion analysis: here, the descent preparation and homing orbits will be assumed coplanar.

The obtainable knowledge of the spacecraft dynamical state on this orbit depends on the observation strategy and the type of comet (density, size). Previous studies[1-4] have demonstrated an estimation accuracy of a few tens of meters in position and a few millimeters per second in velocity. Because of the similarity between the assumptions made in Ref. 2 and those of this paper, its results, shown in Table 5, will be adopted here. It is assumed that the uncertainty ellipsoid has its minor axis coincident with the normal to the orbit and that its intersection with the orbital plane is circular (radial and transverse directions).

Homing Orbit

The purpose of the homing orbit is to bring the spacecraft to a position and velocity that allow the use of onboard instruments to synchronize the spacecraft motion with that of the landing site and initiate the autonomous final descent. Two homing strategies have been developed and used to map the initial errors of Table 5 from the descent preparation orbit until initiation of the final descent, at the synchronization point.

Homing Strategy

At a prestored time t_1, corresponding to angular displacement θ_1 from the apoapsis of the descent preparation orbit (see Fig. 1), the deorbit burn is performed with the 400-N engine. At the end of firing (time t_2), the spacecraft is at an angle θ_2 from the apoapsis of the homing orbit (angles are measured from the antiperiapsis direction for a hyperbolic homing orbit). The descent along the homing orbit is nominally free of orbital maneuvers in order to minimize the dispersions. The spacecraft is rotated from the firing attitude to the landing attitude while onboard inertial measurements coupled with the comet kinematics model uplinked before deorbit ensure the propagation of the estimated spacecraft state relative to the site. At time t_3, the spacecraft arrives at an altitude h_3 (radius r_3) above the selected landing site, with in-plane velocities v_{r3} (radial) and v_{t3} (transverse), where the synchronization maneuver takes place, using the hydrazine thrusters.

The parameters of the homing orbit can be completely defined by its end conditions (at t_3) above the landing site: the velocities v_{r3} and v_{t3} at r_3, the landing site inertial position [right ascension $\alpha_L(t_3)$, declination δ_L from the comet equator], and the azimuth angle β between the transverse velocity vector v_{t3} and the easterly rotational velocity of the landing site. The inclination i_H of the homing orbit (with respect to the comet equator) is related to these parameters with

$$\cos(i_H) = \cos(\beta)\cos(\delta_L)$$

When $\beta = 0$ deg, the inclination of the homing orbit is the same as the latitude of the landing site and the transverse velocity of the spacecraft is parallel to that of the site at t_3. When $\beta = 90$ deg, the orbit is polar.

The relative phasing between the descent preparation and homing orbits is defined by the angle θ_1 at the deorbit point and, along with the in-plane characteristics of the descent preparation orbit (periapsis h_p and apoapsis h_a altitudes), determines the magnitude of the delta-v maneuver.

Table 5 Initial estimation errors (1σ before deorbit maneuver)

Coordinates	Position, m	Velocity, mm/s
Radial	70	0.92
Transverse	70	0.92
Normal	14	0.31

Thus, for a desired synchronization time t_3, a total of nine parameters define the homing orbit and the deorbit delta-v: v_{r3}, v_{t3}, h_3, $\alpha_L(t_3)$, δ_L, β, θ_1, h_p, and h_a. With imposed landing site coordinates and descent preparation orbital parameters (3 $\times$ 15 km), we are left with the quantification of five parameters: v_{r3}, v_{t3}, h_3, β, and θ_1.

Two methods will be used to select these parameters, depending on which of the following two descent strategies is used: 1) slow descent (with laser mapper), and 2) fast descent (without laser mapper). The first strategy (Rosetta baseline scenario) takes into account the constraints imposed by the laser mapping. The second one is an alternate strategy to the situation where the laser mapper has failed in an earlier phase of the mission or when no significant surface features on the comet allow its unambiguous operation in a mapping mode. In this case, only the radar measurements are used for navigation.

Design Constraints: Slow Descent

In the scenario where the laser mapper is functional, the accumulated position errors during homing are measurable and can be cancelled out by the onboard system during final descent. Hence, the minimization of dispersions during homing is not a driving factor, as long as the spacecraft is within the range of the area corresponding to the onboard map (500 $\times$ 500 m) at the end of homing. From a purely GNC point of view, the main design driver is to optimize the operation of the laser mapper. In this context, the following essential (E) and desirable (D) requirements are imposed on the choice of the homing orbit parameters.

Essential Requirement E1

The requirement to map an area of 30-m radius within the $\pm$4-deg laser field of view (see Table 4) imposes a minimum operational altitude of 500 m (with some margin). As a starting assumption, let us specify a minimum of five laser measurement updates (every 200 s) during final descent in order to provide some averaging of the random errors in these measurements. This implies an operational time of at least 1000 s above 500 m, which translates into the following condition on the altitude at synchronization h_3:

$$h_3 \geq 500 + v_d(1000) \tag{1}$$

where the units are in meters and meters per second. Here, v_d is the average descent speed of the spacecraft after synchronization. Its magnitude is constrained by the time allocated for the descent operations (upper limit on time) and by safety considerations (upper limit on vertical speed). It is typically in the range of 0.5–2 m/s. A corresponding minimum altitude range of 1000–2500 km results for h_3. Note that this altitude constraint is consistent with the requirement to avoid contamination of the landing site with hydrazine. In fact, the synchronization delta-v must be completed before the spacecraft reaches an altitude of 200–400 m, at which point actuation switches to the cold gas thrusters.

Evidently, the 30-m radius of the map, the 4-deg laser field of view, the 200-s update period, and the five required updates are parameters that are subject to future refinements. However, it is expected that these assumptions represent conservative estimates.

Essential Requirement E2

Whereas E1 was an operational constraint, the second requirement is a physical constraint: the homing and descent preparation orbits must intersect. Hence, the choice of the final velocity conditions v_{r3}, v_{t3} must be such that the resulting homing orbit has enough energy to intersect the descent preparation orbit, at least at its periapsis of radius r_p. This imposes a physical constraint that can be expressed as

$$v_{t3} \geq v_{\min}(r_3, v_{r3}) \tag{2}$$

where

$$v_{\min} = \{[2\mu_c(1/r_p - 1/r_3) + v_{r3}^2]/(r_3^2/r_p^2 - 1)\}^{1/2} \quad (3)$$

and where μ_c is the comet gravitational parameter.

Desirable Requirement D1

Although a safe periapsis altitude is an essential requirement in the design of the descent preparation orbit, it can no longer be considered mandatory once the descent has been initiated, i.e., for the homing orbit. However, because of possible system failures or if the laser is not able to lock on the selected landing area, it might still be desirable to avoid a collision course, although, this time, with a smaller margin than for descent preparation orbit. Imposing the desirable condition that the periapsis of the homing orbit should be at least a few hundred meters above the comet, we get

$$v_{t3} \geq v_{\text{safe}}(r_3, v_{r3}) \quad (4)$$

where

$$v_{\text{safe}} = \{[2\mu_c(1/r_{pH} - 1/r_3) + v_{r3}^2]/(r_3^2/r_{pH}^2 - 1)\}^{1/2} \quad (5)$$

The periapsis radius r_{pH} of the homing orbit is chosen as $r_{pH} = R_{\max} + 200$ m, where $R_{\max}$ is the maximum comet radius.

Desirable Requirement D2

In order to minimize the dispersions caused by a large synchronization maneuver and to allow an early undisturbed operation of the laser, it would be advantageous to design the homing orbit with final conditions that correspond to the desired initial conditions for the final descent, i.e., corotation of the spacecraft with the landing site and initial vertical velocity equal to the desired average descent speed v_d (0.5–2 m/s):

$$v_{t3} = \omega_c(R + h_3)\cos\delta_L \quad (6)$$

$$v_{r3} = -v_d \quad (7)$$

$$\beta = 0 \text{ deg} \quad (8)$$

where R is the comet radius at the landing site.

Selection of Parameters: Slow Descent

These essential and desirable requirements can be visualized in a single graph, as shown in Fig. 2 for a typical and large comet. The abcissa represents the altitude h_3 above the landing site and the ordinate, the transverse velocity v_{t3} at synchronization. It has been assumed that the desired descent speed v_d is achieved at the end of the homing orbit [i.e., Eq. (7) is satisfied]. Various numerical values for v_d have been investigated, and Fig. 2 represents the least constraining choice for the typical (1 m/s) and large (2 m/s) comet masses. The allowable range for h_3 is specified by requirement E1 [Eq. (1)] and corresponds to the values on the right of the vertical lines (1500-m typical comet, 2500-m massive comet). The allowable values for v_{t3} are determined by three additional curves, corresponding to the essential and desirable constraints E2, D1, and

Table 6 Final homing orbit conditions: typical comet

Parameters	Slow descent (with laser)	Fast descent (without laser)
h_3	2000 m	500 m
v_{r3}	−1.0 m/s	−2.0 m/s
v_{t3}	1.2 m/s	2.5 m/s
Δv_{sync}	0.42 m/s	2.0 m/s
e_H	1.329	4.774
a_H	−8723 m	−594.4 m
h_{pH}	370.7 m	−256.9 m

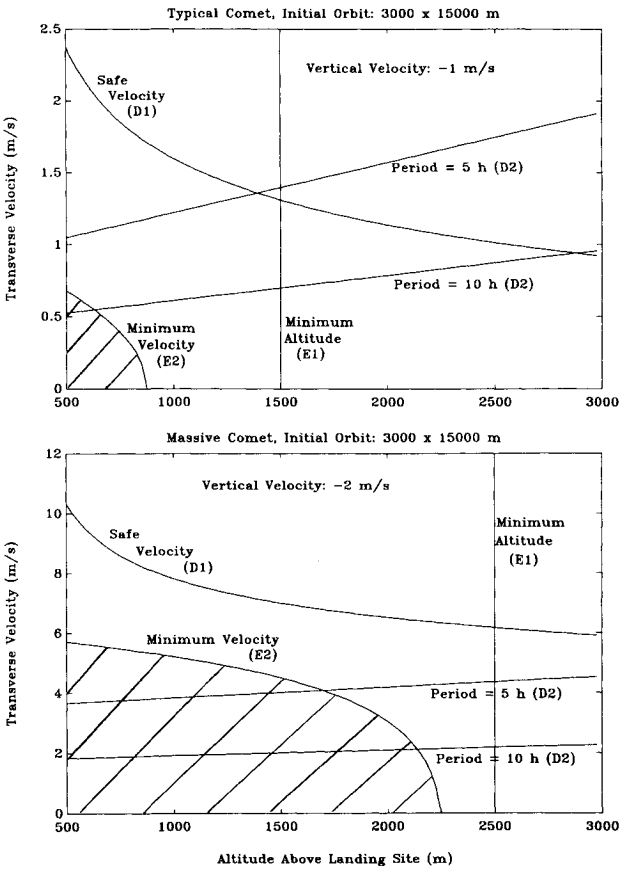

Fig. 2 Design curves for the homing orbit.

D2: 1) minimum physically possible transverse velocity $v_{\min}$, requirement E2, Eq. (3); 2) safe transverse velocity v_{safe}, requirement D1, Eq. (5); and 3) synchronization speed for a comet period of 10 h, requirement D2, Eq. (6) (the synchronization speed for a 5-h comet period is also shown for illustration).

The selection of v_{t3} proceeds as follows: 1) the transverse velocity v_{t3} must be chosen larger than the minimum transverse velocity $v_{\min}$, 2) preferably above the safe velocity v_{safe}, and 3) also preferably close to the synchronization velocity at that altitude for the given comet orbital period. It can be seen from the graphs that, as the comet mass increases, the constraint imposed by $v_{\min}$ (E2) becomes more stringent and a higher altitude h_3 must be selected to achieve synchronization with slowly rotating comets. However, in the two examples shown, it so happens that the laser operational requirement (E1) is the most constraining one ($h_3 > 1500$ m and $h_3 > 2500$ m, respectively). Another observation is that, for small and typical comets, it is possible to achieve both a safe and nearly synchronized transverse velocity, e.g., for a typical comet, $h_3 = 2000$ m and $v_{t3} = 1.2$ m/s with a delta-v of about 0.4 m/s to synchronize with a 10-h period comet. For a massive comet, these two desirable requirements are mutually exclusive (see Fig. 2). In this case, the homing orbit has a large amount of energy that must be distributed between the transverse and radial velocity components. A large transverse velocity (e.g., 6.2 m/s at 2500 m) ensures a safe orbit but the delta-v required for synchronization is also large (delta-v = 4 m/s, requiring a 400-s firing time using two 10-N hydrazine thrusters while the spacecraft travels 800 m horizontally). On the other hand, a large radial velocity allows a more synchronized transverse velocity and an early undisrupted laser operation above the 500- × 500-m landing area but would place the spacecraft on a collision course with the comet during homing.

The parameters selected for further study are shown in the second column of Table 6 (typical comet). The required synchronization delta-v and the nominal eccentricity e_H, semi-

major axis a_H, and periapsis altitude h_{pH} of the homing orbit are also given.

The only parameters that remain to be quantified are the deorbit point θ_1 and the azimuth of the velocity vector β. The obvious selection criteria for the first one would be to minimize the magnitude of the deorbit delta-v, which implies a deorbit maneuver shortly after the apoapsis of the descent preparation orbit ($\theta_1 \simeq 0$ deg). However, the magnitudes involved are relatively small and a more suitable selection criteria would be to minimize the sensitivity to maneuver and model errors. A sensitivity analysis (not reported here) was conducted to determine the impact of the deorbit point θ_1 on the amplification of various errors during homing. Clearly, a deorbit maneuver close to the periapsis ($\theta_1 \simeq 180$ deg) is shown to be preferable and has been selected in the numerical simulations. Therefore, the deorbit burn takes place at 3-km altitude.

Synchronization with the landing site requires that β be zero, in accordance with Eq. (8), and this value is selected in the nominal case. However, in order to see the impact of a large out-of-plane synchronization delta-v, simulations with $\beta = 90$ deg (polar homing orbit) will be conducted.

Selection of Parameters: Fast Descent

Without the laser mapping measurements, minimization of the errors is of primary importance and a fast descent from the 3-km deorbit altitude is preferred to limit the accumulation of model errors. Therefore, in this alternative scenario, a large average velocity along the homing orbit is selected by choosing a large final velocity at the synchronization point: $v_{t3} = 2.5$ m/s, $v_{r3} = -2$ m/s. The altitude at synchronization h_3 is chosen to guarantee enough time to detect a failure, avoid a collision with the comet, and place the spacecraft in a safe orbit, waiting for the ground to take further actions. It is also chosen to ensure the completion of the synchronization delta-v with the more efficient hydrazine thrusters before switching over to the cold gas thrusters, around 200–400-m altitude. Thus, a final homing orbit h_3 of 500 m is selected. The resulting high eccentricity and negative periapsis altitude of this homing orbit are shown in the last column of Table 6, along with the required synchronization delta-v.

Numerical Results (Homing)

A software was developed to generate the homing orbit strategy and to conduct Monte Carlo simulations to propagate the initial estimation errors from the descent preparation orbit to the synchronization point, taking into account the various bias and random errors presented in Tables 2–5. Four types of trajectories are successively propagated by the software: 1) a theoretical trajectory state vector X_t, assuming an impulsive maneuver, used to compute the required delta-v, firing time, and homing time t_3–t_1; 2) a nominal trajectory X_n, integrated from the nominal initial conditions over the fixed homing time, taking into account the finite thrust time; 3) actual Monte Carlo trajectories X; and 4) the associated estimated trajectories $\hat{X}$.

Because of the near-impulsive nature of the 400-N deorbit maneuver (a few seconds duration), the final theoretical and nominal states at synchronization are basically the same. From the nominal estimated state at deorbit time $\hat{X}(t_1) = X_n(t_1)$, the real trajectories X are integrated with the following model errors and disturbances: 1) initial dispersion errors, 2) dipolar gravity field, 3) nongravitational accelerations, 4) attitude errors during firing, and 5) thrust magnitude error.

Similarly, the onboard estimation of the trajectories $\hat{X}$ are generated in parallel, accounting for the following propagation errors: 1) initial estimation errors, 2) spherical gravity model, 3) error in the knowledge of the comet mass, and 4) accelerometer measurement errors. The magnitude of the respective errors are those shown earlier in Tables 2–5.

A sensitivity analysis (not reported here) was performed to investigate the effects of the real-world dipolar gravity model on the dispersion and estimation errors. As expected, the assumption of a spherical gravity model in the estimator and reference trajectory generator introduces biases with respect to the actual trajectories. The standard deviations of the errors, on the other hand, are not significantly affected. Since the dominant gravitational harmonics of the comet gravity field can be determined accurately by the ground navigation process,[3] the contribution of residual model errors in these gravity harmonics will be ignored in the Monte Carlo simulations now described.

Table 7 gives the results of the Monte Carlo simulations in the case of a typical comet. Dispersion and estimation errors are reported along the radial r, transverse t, and normal n directions for both the slow and fast descent scenarios. In all cases, 50 Monte Carlo integrations of the 12 state variables were performed for the fixed homing duration. The errors are more important for the fast descent scenario. This is explained by the fact that, although the rate of descent is faster, the descent time (from 3000 to 500 m) is longer than that of the slow descent scenario (to 2000 m), thereby allowing for a longer accumulation of model errors. The data of Table 7 will be used as initial conditions to the synchronization and final descent closed-loop simulations described in the following.

Final Descent

Contrary to the unguided nature of the homing phase, autonomous closed-loop guidance, navigation, and control operations are implemented for the final descent. The onboard GNC software is designed to operate according to two basic control modes: the synchronization mode and the terminal descent mode. At the predetermined altitude h_3 above the comet (as measured by the radar), the synchronization mode is autonomously activated. Its guidance objectives are to bring the spacecraft along the surface normal at the landing site and to maintain this corotation while the vertical descent speed is controlled to its prestored value (1 m/s in the simulations). The radar and laser measurements are used to refine the onboard knowledge of the landing attitude obtained until now by inertial means. The GNC software operates in this mode until the onboard estimator has converged to within prestored bounds. If the spacecraft descends below a given altitude (700 m in the simulations) while the estimated position errors are still too large, its descent speed is exponentially decreased to zero until convergence is achieved.

When these mode transition conditions are satisfied, the terminal descent mode is initiated. The vertical descent speed is maintained (or reacquired) and the estimated horizontal position errors are actively controlled to zero. At 400 m (nominally) from the surface, actuation is switched from hydrazine to cold gas thrusters in order to avoid contamination of the sampling site. At 175 m, the spacecraft descent is braked, aiming at 10-cm/s vertical speed at touchdown, while horizontal speed is controlled to zero.

The autonomous GNC system has been described in an earlier paper[7] and only its major characteristics are presented here.

Table 7 Errors (1σ) at synchronization: typical comet

	Dispersion		Estimation	
Axes	Slow	Fast	Slow	Fast
	Position, m			
r	74.0	80.5	72.1	72.8
t	80.2	86.7	78.5	78.2
n	18.0	35.5	11.6	11.5
	Velocity, mm/s			
r	17.6	37.2	14.4	14.6
t	19.6	35.4	14.1	17.2
n	11.1	29.3	0.4	0.8

Navigation

In the baseline descent scenario, the available onboard measurements are the altitude, the surface normal, the relative velocity, the horizontal position (laser maps), and the nongravitational accelerations. A total of eight state variables are propagated: six translational states (position and velocity) and two attitude-angles (unit vector normal to comet surface). In the backup scenario where the laser mapper is not available, the horizontal position is predicted with the onboard models. The performance of the related instruments have been discussed earlier (Table 4) and their assumed operational profile is summarized in Table 8.

Innovations in the state vectors based on the measurements are computed every second, using the estimated state vector along the unobservable coordinates (pseudomeasurements). These innovations are fed into a second-order, linear observer with gains that are scheduled according to the guidance mode of operation (synchronization or terminal descent). These state estimates are expressed in inertial coordinates. Their transformation into estimates relative to the landing site reference frame is computed using the onboard knowledge of the comet state, which has been propagated since the deorbit maneuver, when the comet kinematics parameters and landing site coordinates were last uplinked to the spacecraft.

Guidance and Control

The guidance laws are composed of prestored phase-plane trajectories made of a combination of constant position, constant velocity, constant braking, and exponential braking profiles in all three axes, one set of phase-plane trajectories for each of the synchronization and terminal descent modes. Control commands are computed with classical proportional-derivative laws, using as error signal the difference between the estimated state and that computed from the reference phase planes. Here again, two sets of control gains are prestored in the onboard computer, one for each of the descent control modes.

Numerical Results (Final Descent)

The basic software for the simulation of the guided descent has been developed and coded by MATRA and INISEL ESPACIO under contract by ESA.[6] Modifications were later performed within ESA to incorporate new instruments (laser mapper, accelerometers), additional external disturbances (solar pressure, thruster leaks, comet outgassing), new guidance modes, and new utilities (capability for Monte Carlo simulations, computation of propellant consumption, etc.). Block diagrams of the real-world simulator and onboard GNC software are shown in Figs. 3 and 4, respectively. Using this software, a Monte Carlo analysis was conducted to evaluate the obtainable landing accuracy to a site located on the comet equator. Three different cases are studied: A) slow descent strategy using the laser mapper, with final transverse velocity on the homing orbit in the same direction as the landing site velocity (i.e., β = 0 deg and homing orbit inclination = landing site latitude = 0 deg); B) same as case A, but with final transverse velocity on the homing orbit perpendicular to the landing site velocity (i.e., β = 90 deg, and homing orbit inclination = 90 deg); and C) fast descent strategy from 500 m, without laser mapper, with β = 0 deg.

As initial conditions for the final descent, the estimated state of Table 7 at the end of the homing orbit is assumed. In addition to these random initial conditions, each Monte Carlo simulation is started with different random values for the comet kinematics parameters, for the comet gravitational parameter, and for the onboard knowledge of the spacecraft mass and landing site coordinates. Each simulation also has a different sequence of random numbers for the modeling of external disturbances, attitude/pointing errors, and measurement errors of each instrument. The associated standard deviations assumed in the simulations are those presented in Table 2 (comet), Table 3 (dynamics), and Table 4 (measurements).

The results of the simulations are compiled in Table 9. The total descent time from synchronization to landing is about 40 min for cases A and B (from 2000 m) and 15 min for case C (from 500 m). These results show that, while random errors tend to be averaged out by the laser map measurements, the biases in the measurements and models significantly affect the landing accuracy. Ground and onboard estimation of these biases (now under investigation) would greatly improve the landing accuracy. A homing orbit that contains the velocity vector of the landing site at the time of synchronization (case A: β = 0 deg) tends to minimize the dispersions when compared to a polar approach (case B) since a lower thrusting effort is required to achieve synchronization. Laser-assisted navigation (cases A and B) provides much better performance

Table 8 Instruments operational profile

Measurements	Range, m	Update frequency, Hz
Laser maps	5000-500	0.005
Altitude	5000-20	1
Normal	2000-20	1
Velocity	2000-20	1
Accelerations	—	1

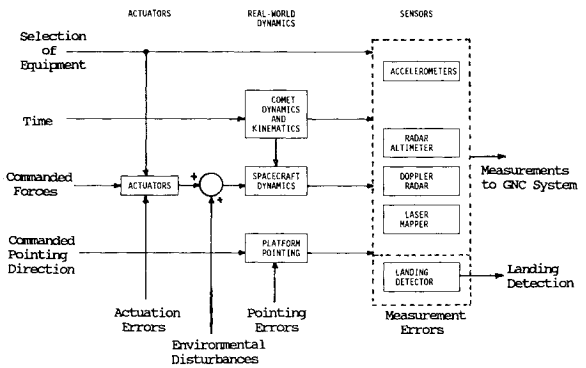

Fig. 3 Dynamics, kinematics, and equipment simulator.

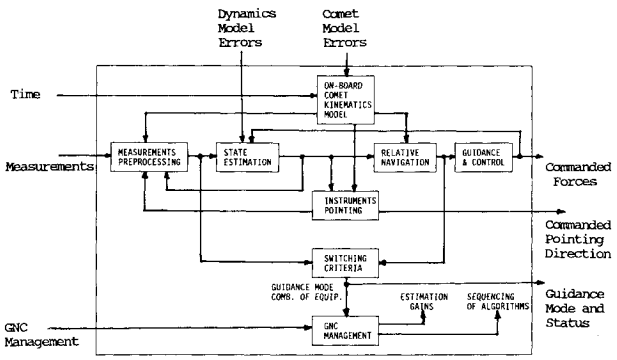

Fig. 4 Onboard GNC system.

Table 9 Landing accuracies

	Case A	Case B	Case C
	Bias errors, m		
East	14.6	17.5	21.4
North	−14.5	−16.0	−13.6
	Random errors, 1σ m		
East	2.3	11.8	70.0
North	1.1	2.4	15.6
	Total rms errors, m		
East	14.8	21.1	73.2
North	14.5	16.2	20.7

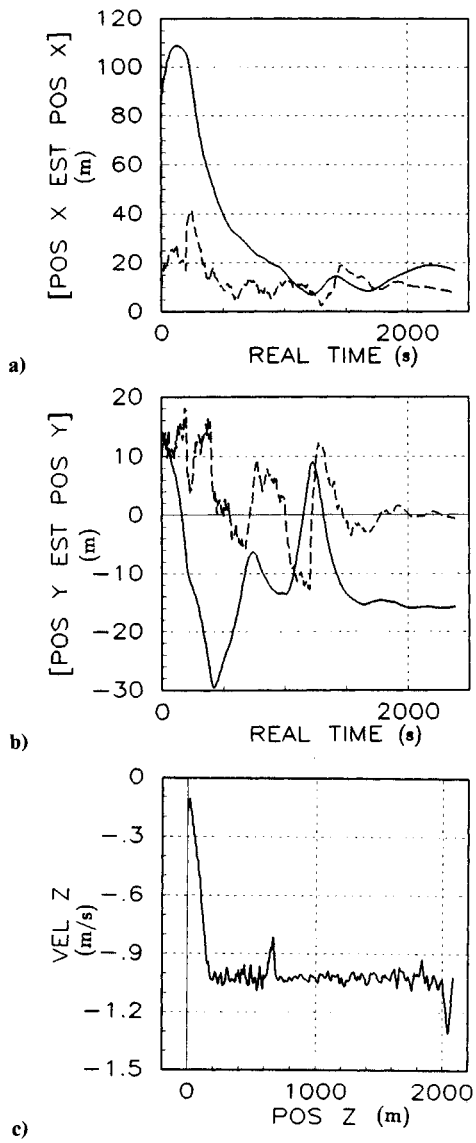

Fig. 5 Descent simulation with laser.

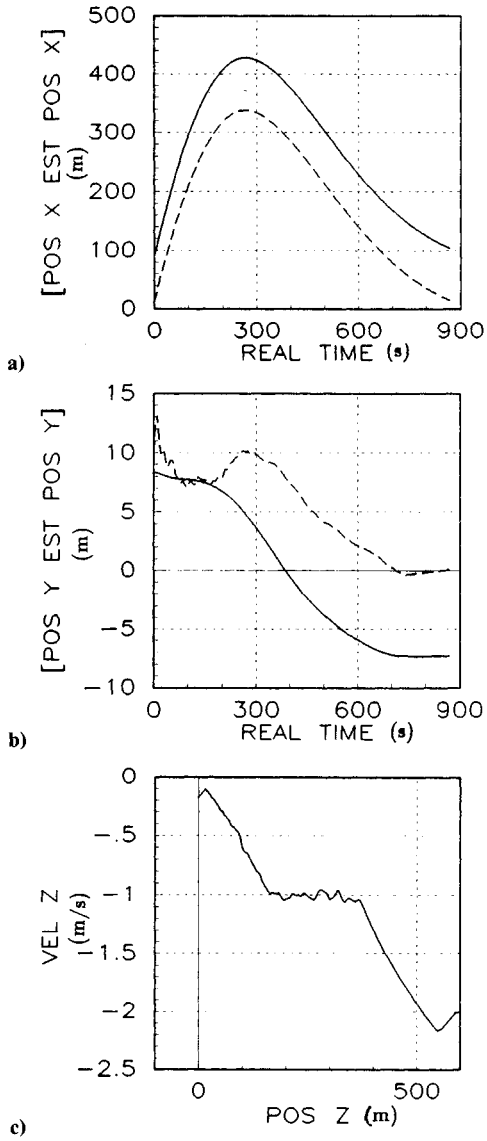

Fig. 6 Descent simulation without laser.

than radar-only navigation (case C), as expected. Nevertheless, even without laser assistance, the landing errors are still below 80 m (rms).

In addition to accuracy, another important characteristic of the touchdown is its safety, expressed here as the magnitude of the horizontal and vertical velocity of the spacecraft. The nominal touchdown conditions programmed in the guidance algorithm are zero horizontal velocity and a 10-cm/s vertical impact speed. Table 10 shows the touchdown velocity for case A and demonstrates a performance better than 3 cm/s (rms) along each axis.

A typical simulation of case A is shown in Fig. 5. Figures 5a and 5b give the real (solid line) and estimated position of the spacecraft in the east-west (X) and north-south (Y) directions. For case A (β = 0 deg), these correspond to in-plane and out-of-plane directions, respectively (equatorial orbit). The laser map updates every 200 s can be observed, especially in the north-south direction where the end of laser operation around 1500 s (at 500 m, see Table 8) is responsible for the large final error. Figure 5c shows the phase plane trajectory of the spacecraft altitude. As commanded by the prestored guidance laws, the descent velocity is kept at -1 m/s until an altitude of 175 m, at which point it is commanded to -10 cm/s. The slight reduction in descent speed, visible at 700 m, has occurred because the horizontal estimated errors were still too large for the terminal descent mode to be initiated. Exponential braking was commanded until convergence allowed the initiation of the terminal descent mode and the reacquisition of the 1-m/s descent speed.

Table 10 Landing velocity (rms, mm/s)

East	21.9
North	8.4
Vertical	129.7

The equivalent graphs for case C (no laser) are shown in Fig. 6. The absence of horizontal position measurement is evident: the initial position errors at synchronization (Table 7) are not compensated during the guided descent. Because of these relatively large landing errors, the autonomous detection of a safe landing area using the radar roughness measurements might be necessary and is presently under investigation at ESA. It can be observed from Fig. 6c that the spacecraft vertical velocity of -2 m/s at synchronization is braked to -1 m/s during the guided descent.

Conclusions

This paper has described and analyzed the autonomous GNC operations required to safely land a spacecraft on a cometary body. The initial uncertainty in the spacecraft position and velocity has been propagated from the descent preparation orbit until touchdown, taking into account the errors in the onboard comet model, the effects of environmental disturbances, and those of measurement/actuation errors. Monte

Carlo simulations of three types of descent have been performed: two that rely on laser mapping for position measurement (with polar and equatorial descent planes) and one without the assistance of the laser mapper. It is demonstrated that, with the laser mapping technique and a synchronized descent orbit, the landing accuracy is of the order of 20-m bias and 7-m random (3σ). When the equatorial landing site is approached from a polar orbit, the landing accuracy is degraded to 24-m bias and 36-m random (3σ) because of the large out-of-plane delta-v maneuver required for synchronization. The estimation of the biases in the models and measurements would clearly improve the landing accuracy. In the event of a laser system failure, a backup scenario using radar measurements alone allows a landing accuracy of the order of 25-m bias and 215-m random (3σ). In this case, the autonomous detection of, and guidance to, a safe (flat) area using the radar could be useful and is now being investigated. The paper has also demonstrated that the guidance and control laws ensure a safe touchdown velocity: below 3 cm/s (rms) in the horizontal plane and up to 13 cm/s vertically.

Acknowledgments

The author gratefully acknowledges the work of V. Guillaud and M. Caldichoury of MATRA and A. Ferigle and L. Cabré of INISEL ESPACIO in the development of the guided descent simulation software.

References

[1]Miller, J. K., "Navigation of the Landing of a Spacecraft on a Comet Nucleus," Jet Propulsion Lab., CNSR/JPL TN 23, Pasadena, CA, Jan. 1990.

[2]Bello-Mora, M., "On the Rosetta Comet Approach Phase Orbit Strategy and Navigation," European Space Operations Centre, MAS Working Paper 309, Darmstadt, Germany, June 1990.

[3]Miller, J. K., Weeks, C. J., and Wood, L. J., "Orbit Determination of the Comet Rendezvous/Asteroid Flyby Mission: Post-Rendezvous Phases," AIAA Paper 89-0348, Jan. 1989.

[4]Miller, J. K., and Wood, L. J., "Navigation of the Mariner Tempel 2 Mission: Orbit Phase and Penetrator Development," AIAA Paper 87-0092, Jan. 1987.

[5]Anon., "Study and Design of a Comet Approach and Landing System," Draft Final Rept., Officine Galileo, European Space Agency Contract 7988/88/NL/PB(SC), June 1990.

[6]Anon., "Autonomous and Advanced Navigation Techniques Study," Final Rept., MATRA Espace, European Space Agency Contract 7562/88/N-L/MAC, April 1989.

[7]Guillaud, V., and de Lafontaine, J., "Navigation in the Vicinity of a Cometary Nucleus," American Astronomical Society/Goddard Space Flight Center International Symposium on Orbital Mechanics and Mission Design, AAS-89-207-1, Goddard Space Flight Center, Greenbelt, MD, April 1989.